

# Nonlinear Adaptive Control of Optical Jitter with a New Liquid Crystal Beam Steering Device

Pawel K. Orzechowski, Steve Gibson and Tsu-Chin Tsao

Mechanical and Aerospace Engineering  
University of California, Los Angeles  
Los Angeles, CA 90095-1597

Dan Herrick and Victor Beazel

Optics Division, AFRL/DES  
Directed Energy Directorate  
U.S. Air Force Research Laboratory  
Kirtland AFB, NM 87117-5776

Milind Mahajan, Bing Wen and Bruce Winker

Teledyne Scientific Company  
1049 Camino Dos Rios, Thousand Oaks, CA 91360

**Abstract**—This paper presents a new approach to active control of optical jitter with a new transmissive liquid crystal beam steering device, or tilt corrector. The device is driven by a linear time-invariant feedback control loop and an adaptive control loop to maximize the jitter-rejection bandwidth. In contrast to conventional fast steering mirrors, the liquid crystal device optically redirects the laser beam. The new device has no moving parts and requires low operating power. The paper presents experimental results that demonstrate the capabilities of the liquid crystal device and the adaptive controller to suppress high-bandwidth jitter. For the control system, the liquid crystal device presents nonlinearities due to a rate limit and quantization. The experimental results show the importance of modeling the nonlinearities in the adaptive controller.

*Index Terms:* Control of lasers, optical jitter, adaptive control, liquid crystal beam steering device

## I. INTRODUCTION

Laser beam steering plays a central role in contemporary technological applications such as free-space optical communications, high-energy laser (HEL) systems, scanning optical lithography and laser welding and cutting. These applications demand precise pointing of laser beams in environments where disturbances like platform vibration and atmospheric turbulence induce laser beam jitter that poses critical performance limitations. Typical disturbances have multiple bandwidths, both broad and narrow, that vary with time. High-performance control of non-stationary optical jitter requires advanced control methods.

Recent research has developed novel adaptive control methods that can track and reject non-stationary, high-bandwidth jitter in laser beams. These methods combine adaptive filters that implicitly track disturbance characteristics with feedforward and/or feedback control laws that drive actuators to suppress jitter. The adaptive filtering methods

used include least-mean-square (LMS) adaptive filtering [1]–[5] and recursive least-squares (RLS) adaptive filtering [6]–[13]. In all of this research, fast steering mirrors (FSM) were used to steer the laser beams.

In the research described in this paper, a new transmissive liquid crystal beam steering device developed by Teledyne Scientific Company of Thousand Oaks, CA, replaces the classical fast steering mirror as the control actuator. Because the liquid crystal device has no moving parts and requires low operating power, it is a potentially attractive alternative to fast steering mirrors for line-of-sight beam stabilization.

The beam control experiments described in this paper were conducted in UCLA's beam control laboratory, in collaboration with the researchers from the Air Force Research Laboratory (AFRL) and Teledyne Scientific Company. Preliminary experimental results were reported in [14], [15]. The results in this paper are taken from [16].

The experiments employed a variable-order adaptive controller based on a recursive least-squares (RLS) lattice filter. Adaptive control schemes similar in structure to the adaptive controller here have been used in [7]–[13] for control of fast steering mirrors with significantly different dynamic characteristics from those of the liquid crystal beam steering device here, and in recent papers on adaptive optics [17]–[20] where many sensor and control channels were used. The novel feature of the adaptive controller here is the use of the nonlinear plant model to represent the nonlinearities in the liquid crystal device. Experimental results in this paper show that, for sufficiently large disturbance amplitude, representing the plant nonlinearities in the adaptive controller is essential for good performance.

## II. TRANSMISSIVE LIQUID CRYSTAL TILT CORRECTOR

### A. Tilt Corrector Performance Description and Trade-offs

The transmissive liquid crystal tilt corrector was developed by Teledyne Scientific Company (TSC) of Thousand Oaks, CA. The liquid crystal tip-tilt corrector leverages dual frequency liquid crystal optical phased array (OPA) technology

This work was supported by the U.S. Air Force Office of Scientific Research under Grant F49620 02 01 0319 and the U.S Naval Office of Research under Grant N00014 07-1-1063.

Pawel K. Orzechowski is currently with Northrop Grumman Space Technology, Controls System Department, Redondo Beach, CA.

[21] to address the need for a compact, transmissive, high-speed tip-tilt correction device in a laser electro-optic system. The primary difference between the tip-tilt corrector and other optical phased arrays is that tip-tilt corrector does not have phase resets across the aperture. Teledyne uses dual frequency liquid crystals (DFLCs) [22], [23] for high-speed steering applications in the near infrared because this class of materials surpasses all others in terms of switching speed, phase stability and electronic controller size, weight and power. The physics and design of the liquid crystal device are discussed in more detail in [14].

The 2 cm aperture transmissive tip-tilt corrector has  $\pm 300 \mu\text{rad}$  field of regard in both directions,  $2 \mu\text{rad}$  steering resolution, 3.125 kHz frame rate and 24 mrad/sec slew rate. This design offers the following advantages over a fast steering mirror of similar aperture and bandwidth:

- 1) No moving parts, which increases tilt corrector durability and eliminates the need for reaction compensation;
- 2) Transmissive architecture, which significantly reduces coupling of platform vibration and optical performance, since the liquid crystal device has no mechanical dynamics;
- 3) Lithographic fabrication and simple assembly process, which significantly reduce recurring costs;
- 4) Low voltage operation, which significantly reduces controller size, weight and power.

To steer the beam on one axis, 60 individual commands must be sent to three 20-pixel liquid crystal cells. Thus, 120 signal channels, or three 40-channel multi-chip controller modules (MCMs), are required to steer the beam in two dimensions. Teledyne fabricated a 160-channel driver using four 40-channel multi-chip dual frequency drive modules that can accept new voltage and frequency data at a 3.125 kHz frame rate over a 16 bit parallel digital bus.

To eliminate the need for end users to understand dual frequency liquid crystal physics and the low-level programming of the DFCLC driver, Teledyne developed a device controller based on a Blackfin 537 processor. The device controller allows user-friendly high-level control of the tilt corrector by a system level controller (xPC Target in this paper). The device controller accepts an 8-bit parallel digital control signal that commands the controller to increase or decrease the current deflection along X and Y-direction by a certain angle (up to  $8 \mu\text{rad}$ , in steps of  $2 \mu\text{rad}$ ). The device controller then selects the appropriate cell that is ready to accept an angle update and commands the cell to go to a new deflection using appropriate calibration data. The device controller generates the 16-bit command and sends it to the 160-channel driver. Also, the device controller returns a digital timing output to synchronize the system controller with the tilt corrector driver. The DFCLC driver and the device controller are discussed in more detail in [14].

### III. EXPERIMENTAL SETUP

The beam steering experiment, shown in Figs. 1 and 2, includes the following optical components: a 980nm laser, a wire grid linear polarizer, the liquid crystal beam steering

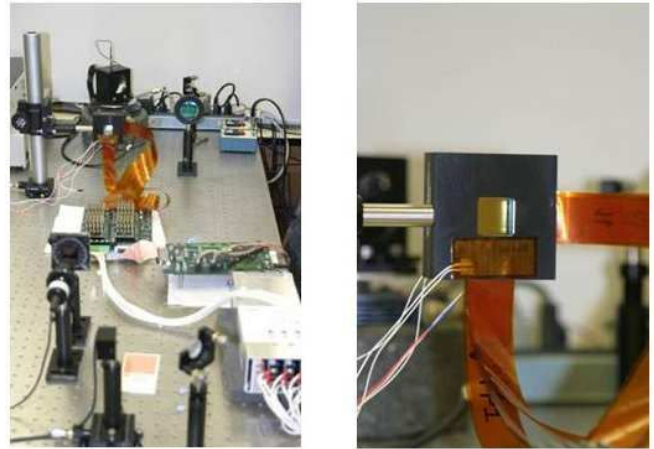


Fig. 1. Laser beam steering experiment. Left: the liquid crystal beam steering experiment. Right: zoomed-in picture of Teledyne's liquid crystal beam steering device.

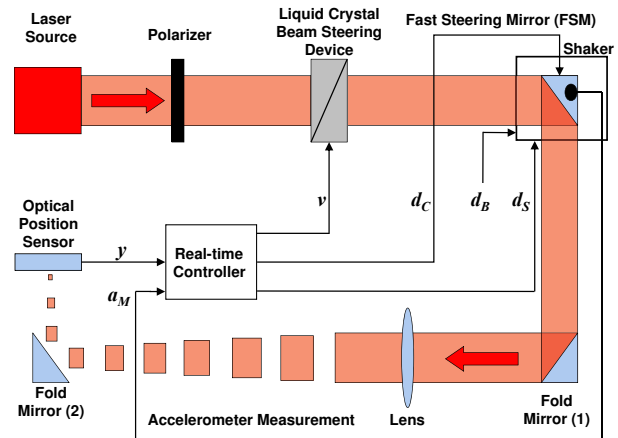


Fig. 2. Diagram of the experiment.

device, a fast steering mirror (FSM) mounted on a shaker, a rigid folding mirror, a convergent lens, followed by a second rigid folding mirror and an optical position sensor (OPS).

MATLAB's xPC Target real-time software processes the control algorithms on a 3.6 GHz Pentium operating at the sample-and-hold rate of 3125 Hz, which is determined by the liquid crystal device's driver electronics. The inputs to the controller are the position of the laser spot on the plane of the sensor, denoted by the two-dimensional vector  $y$ , and the scalar measurement  $a_M$  from an accelerometer mounted on top of the case for the fast steering mirror. The output of the controller is the two-dimensional command vector  $v$  sent to the liquid crystal device.

There are three independent sources of jitter, denoted by  $d_B$ ,  $d_C$ ,  $d_S$  in Fig. 2. The shaker on which the fast steering mirror is mounted responds to building vibration denoted by  $d_B$ . The fast steering mirror and the shaker are driven by the commands  $d_C$  and  $d_S$ , respectively, which are generated in xPC Target but not given to the control loops.

### IV. CONTROL MODEL OF THE LIQUID CRYSTAL DEVICE AND DRIVE ELECTRONICS

The block diagram in Fig. 3 represents the liquid crystal device, along with the DFCLC driver and TSC device con-

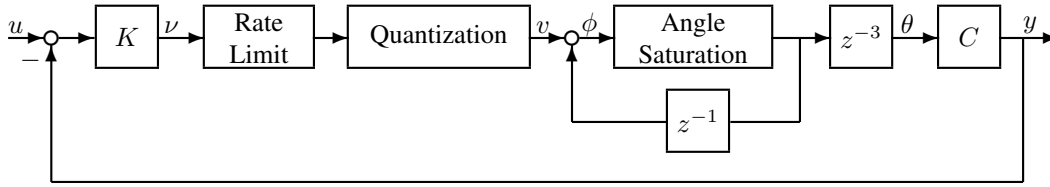


Fig. 3. Block diagram of the liquid crystal device and LTI feedback control loop. The signals (all two-dimensional):  $y$  = measurement vector from optical position sensor,  $\theta$  = beam angle vector,  $\nu$  = net control command before saturation and quantization,  $v$  = slew-rate command to the LC device,  $u$  = feedforward adaptive control command. Constant matrices:  $K$  = diagonal feedback control gain,  $C$  = diagonal matrix of conversions factors.

troller, with the linear-time-invariant (LTI) feedback control loop closed. The liquid crystal device, DFCL driver and TSC device controller are represented by the angle saturation block and the delay blocks with  $z^{-1}$  and  $z^{-3}$ . The input to the TSC device controller is the two-dimensional rate command  $v$  from xPC Target, and the output of the liquid crystal device is the pair of beam angles in the vector  $\theta$ . The three delays represented by the  $z^{-3}$  block are due to the electronics in the DFCL driver and TSC device controller and the response time of the liquid crystal device. The  $z^{-1}$  block represents the fact that the DFCL driver and the liquid crystal device integrate the rate command.

The TSC device controller receives commands at the rate of 3125 Hz. These slew-rate commands, denoted by the two-vector  $v$ , are limited to integer values between -4 and +4; hence the rate limit and quantization blocks in Figure 3. The liquid crystal device can steer the beam to 301 discrete states in the range of  $\pm 300 \mu\text{rad}$ . While the device's state transition occurs rapidly within each sample-and-hold interval (1/3125 sec), the quantization and saturation limits on angle and slew rate pose limits on resolution and dynamic response.

The saturation blocks in Fig. 3 are characterized by the following for each axis ( $i = 1, 2$ ):

$$\text{Rate Limit Output} = \begin{cases} \nu_i, & |\nu_i| \leq 4, \\ 4, & \nu_i > 4, \\ -4, & \nu_i < -4, \end{cases} \quad (1)$$

$$\text{Angle Saturation Output} = \begin{cases} \phi_i, & |\phi_i| \leq 150, \\ 150, & \phi_i > 150, \\ -150, & \phi_i < -150. \end{cases} \quad (2)$$

The quantization block in Fig. 3, rounds the input to the nearest integer value, so that the entries in the vectors  $\phi$  and  $\theta$  take integer values, with each integer value  $k$  representing an angular beam displacement of  $2k \mu\text{rad}$ .

The gain matrix  $C$  in Fig. 3 converts the beam angles  $\theta$  to the position measurements  $y$  given by the optical position sensor (OPS). To determine  $C$ , the liquid crystal beam steering device was driven with an open-loop white-noise sequence  $\nu$  (without the control loops closed). The resulting output sequences showed that, as expected,  $C$  is diagonal. A least-squares fit between the input and output data yielded  $C = \text{diag}[0.0130 \ 0.0185]$ .

## V. LTI FEEDBACK CONTROL LOOP

The linear time-invariant (LTI) feedback loop is the control loop in Fig. 3 that maps  $y$  to  $\nu$ . The LTI feedback gain matrix is  $K = \text{diag}[2 \ 2]$ . The LTI feedback loop stabilizes the closed-loop system (without the adaptive controller) and approximately maximizes the error-rejection bandwidth with minimal amplification of high-frequency disturbance. Attempting to increase the bandwidth by increasing  $K$  would produce greater amplification of high-frequency disturbance and sensor noise.

Since the plant has the integral action indicated in Fig. 4, the LTI feedback loop rejects any biases. In this paper, the LTI feedback loop always is closed. Therefore, the output signal  $y$  has zero mean throughout this paper, so that the RMS value and standard deviation of  $y$  are the same in steady-state.

When the LTI feedback loop is closed, there exist stable nonlinear transfer functions  $G$ ,  $G^{yC}$ ,  $G^{yS}$  and  $G^{yB}$  such that

$$y = Gu + w, \quad (3)$$

where

$$w = G^{yS}d_S + G^{yB}d_B + G^{yC}d_C. \quad (4)$$

The output disturbance  $w$  represents the combined effect of the jitter commands  $d_C$  and  $d_S$  and the building vibration  $d_B$ , filtered through the closed-loop transfer functions in (4). As shown in Fig. 4,  $d_S$  and  $d_B$  drive the shaker, and  $d_C$  drives the disturbance fast steering mirror (FSM in Fig. 4). Any sensor noise associated with the optical position sensor would be added to the right side of (4); however, careful measurements of the output of the OPS have shown that sensor noise is negligible in the experiments reported here.

The transfer functions in (3) and (4) are the true system transfer functions, which are not known precisely. Experimental results confirm that  $G$  is essentially diagonal; i.e., steering the beam about one axis with the liquid crystal device produced negligible rotation about the other axis. Therefore,  $G$  is assumed to be diagonal for control design. Fig. 3 defines a nonlinear transfer function  $\hat{G}_{NL}$  from  $u$  to  $y$ . This is an approximation to the true  $G$ .

When the rate limit, angle saturation and quantization are ignored, Fig. 3 yields a linear model of the liquid crystal device with the LTI feedback loop closed. This model is denoted by the linear transfer function  $\hat{G}$ . The Bode plots for the linear sensitivity transfer function  $S = I - \hat{G}$ , from output disturbance to output error with the LTI feedback loop

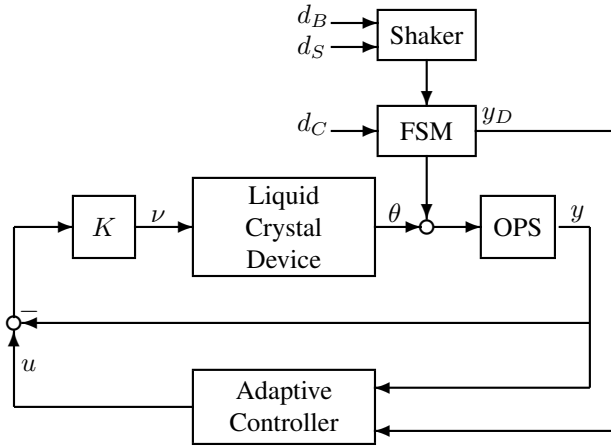


Fig. 4. Block diagram of the complete system.  $d_S$  = disturbance command to shaker;  $d_B$  = building vibration;  $d_C$  = disturbance command to FSM;  $d_M$  = response of FSM;  $\theta$  = beam angle from liquid crystal beam steering device;  $y$  = beam position on sensor;  $y_D$  = accelerometer measurement;  $u$  and  $\nu$  = control commands.

closed, indicate that the LTI feedback loop produces a 6dB jitter-rejection bandwidth of approximately 60 Hz—when the linear model is sufficiently accurate.

## VI. ADAPTIVE CONTROL LOOP

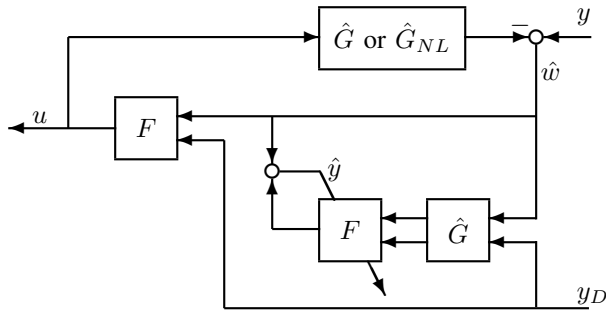


Fig. 5. Block diagram of the adaptive controller.  $\hat{G}$  and  $\hat{G}_{NL}$  are the discrete-time linear and nonlinear estimates of the true plant  $G$ ;  $F$  = multi-input FIR lattice filter;  $\hat{w}$  = estimate of the disturbance sequence  $w$ ;  $\hat{y}$  = sequence to be minimized;  $y_D$  = feedforward measurements.

The block diagram of the adaptive controller is shown by Fig. 5. The adaptive controller feeds back the two-channel beam position error  $y$ , and it can feed forward an arbitrary number of additional sensor signals represented by  $y_D$  in Figs. 4 and 5. Here,  $y_D$  is the accelerometer signal.

Fig. 5 illustrates two alternative methods for generating the estimate  $\hat{w}$  of the output disturbance  $w$  in (4). The sequence  $\hat{w}$  is based either on the LTI representation of  $G$ , denoted by  $\hat{G}$ , or the nonlinear estimate  $\hat{G}_{NL}$ . Hence  $\hat{w}$  can be constructed in either of the following two ways:

$$\hat{w} = y - \hat{G}u, \quad (5)$$

$$\hat{w} = y - \hat{G}_{NL}u. \quad (6)$$

Experimental results in Section VII show that, for sufficiently large disturbance amplitude, the performance of the adaptive controller is much better with (5) than with (6).

The main component of the adaptive controller is the recursive-least-squares (RLS) adaptive filter  $F$  in Fig. 5. This filter has finite impulse response (FIR) and order  $N$ . The adaptive filter has the lattice realization in [24]. The order-recursive structure of the lattice filter allows the adaptive controller here to have variable order. The lattice filter generates adaptive control commands of all orders  $n \leq N$ . During adaptation, lattice-filter orders  $n < N$  are used, with the order increasing to the maximum order  $N$  in steady-state. For the results in this paper,  $N = 60$ . The improved transient response provided by lattice-filter based variable-order adaptive control is discussed in detail in [10], [13].

The lattice filter implicitly tracks the statistics of the disturbance and identifies gains to minimize approximately the RMS value of the output error signal  $y$ . The precise least-squares criterion minimized by the lattice filter  $F$  is the RMS value of the sequence  $\hat{y}$ , as indicated by the slanted arrow in Fig. 5. This tuning signal is given by

$$\hat{y} = \hat{w} + F\hat{G} \begin{bmatrix} \hat{w} \\ y_D \end{bmatrix}. \quad (7)$$

Since the two channels of the plant are modeled as uncoupled for control design, the LTI and adaptive control loops for the two plant channels are uncoupled. In each channel then, the scalar transfer function  $\hat{G}$  commutes with  $F$ . If  $\hat{G} = G$ , the tuning signal becomes  $\hat{y} = y$ . Using the fact that  $\hat{G}$  and  $F$  commute so that the adaptive filter can minimize the  $\hat{y}$  in (7) instead of  $y$  often is referred to as the “filtered- $x$ ” method [25], [26].

## VII. EXPERIMENTAL RESULTS

This section presents results from two experiments. In the first experiment, the adaptive controller used the linear plant model  $\hat{G}$  to generate the estimated disturbance sequence  $\hat{w}$  as in Fig. 5 and (5). In the second experiment, the adaptive controller used the nonlinear plant model  $\hat{G}_{NL}$  to generate  $\hat{w}$  as in Fig. 5 and (6). The experimental results compare the disturbance rejection capabilities of the LTI feedback control loop and of the two versions of the adaptive control loop.

Each experiment was approximately 90 seconds long. In each experiment, LTI feedback control loop was always closed, and only the LTI feedback loop was closed during the first 19 seconds. Then, at  $t = 19$  seconds, the adaptive filter began running. The adaptive control loop remained open during the first 100 steps after  $t = 19$  seconds while the adaptive filter calculated initial estimates of the optimal gains. Then the adaptive control loop was closed with the initial lattice filter order  $n = 4$ , and the order was increased incrementally until the final order  $N = 60$  was reached after 600 steps = 0.2 seconds.

Table I lists the disturbance bandwidths for the three jitter sources. The jitter commands  $d_C$  and  $d_S$  are produced by passing white noise sequences through band-pass filters in xPC Target. (As stated earlier, these command sequences are not given to the control loops.) In Table I and all subsequent results, Axis 1 and Axis 2 refer to the directions in which the

TABLE I  
JITTER SOURCES FOR AXIS 1 AND AXIS 2

Jitter Bandwidths Axis 1	Source
0 Hz–20 Hz	Response to building vibration $d_B$
Jitter Bandwidths Axis 2	Source
0 Hz–20 Hz	Response to building vibration $d_B$
20 Hz–50 Hz pass band	Command $d_C$ to Fast Steering Mirror
99 Hz–101 Hz pass band	Command $d_S$ to Shaker
399 Hz–401 Hz pass band	Command $d_S$ to Shaker
1399 Hz–1401 Hz pass band	Command $d_C$ to Fast Steering Mirror

laser spot is measured on the optical position sensor. Axis 1 is horizontal, and Axis 2 is vertical.

Fig. 6 shows the output errors for the two experiments, and Table II compares steady-state RMS values of the output errors. For the results presented in this paper, the two components of the output error  $y$  measured by the optical position sensor are converted to  $\mu\text{rad}$  according to the discussion in Section IV.

The jitter on Axis 1 has smaller amplitude and bandwidth than than on Axis 2 because the disturbances from the disturbance mirror and the shaker act mainly on Axis 2. For Axis 1, the two versions of the adaptive controller yield similar performance. The difference in Axis 1 RMS values in Table II between adaptive control with  $\hat{G}$  and adaptive control with  $\hat{G}_{NL}$  likely are due to the fact that the building vibration and shaker response are not precisely repeatable.

On Axis 2, the adaptive controller with (6), which uses the nonlinear plant model  $\hat{G}_{NL}$ , significantly outperforms the adaptive controller with (5), which uses the linear plant model  $\hat{G}$ . The amplitude of the output error produced by the adaptive controller with (5) is  $300 \mu\text{rad}$ , the maximum beam deflection achievable by the liquid crystal device. The large output errors result from the difference between the true disturbance  $w$  and the approximation  $\hat{w}$  in (5). With larger jitter magnitude, the nonlinear effects in the liquid crystal device are more significant and must be modeled in the adaptive controller. Table II shows that the adaptive controller with (6) reduces the Axis 2 output error by more than 50% from the output error with LTI feedback only.

The plots in Fig. 6 illustrate important characteristics of the experimental performance of the adaptive controller: fast convergence, control of both broad-band and narrow-band jitter over a wide frequency range, including a reduction greater than 15 dB of the high frequency peak at 1400 Hz.

Fig. 7 shows the input commands to the rate limit in (1) and Fig. 3, for the two versions of the adaptive controller. For Axis 2, both input sequences often exceed the constraint of  $\pm 4$ , so that the constraint is binding, but the adaptive controller with (6) results in a well-behaved rate limit input because the plant model  $\hat{G}_{NL}$  includes the rate limit.

## VIII. CONCLUSIONS

This paper has demonstrated the use of a new liquid crystal beam steering device for closed-loop control of optical jitter. The liquid crystal beam steering device performs two-axis

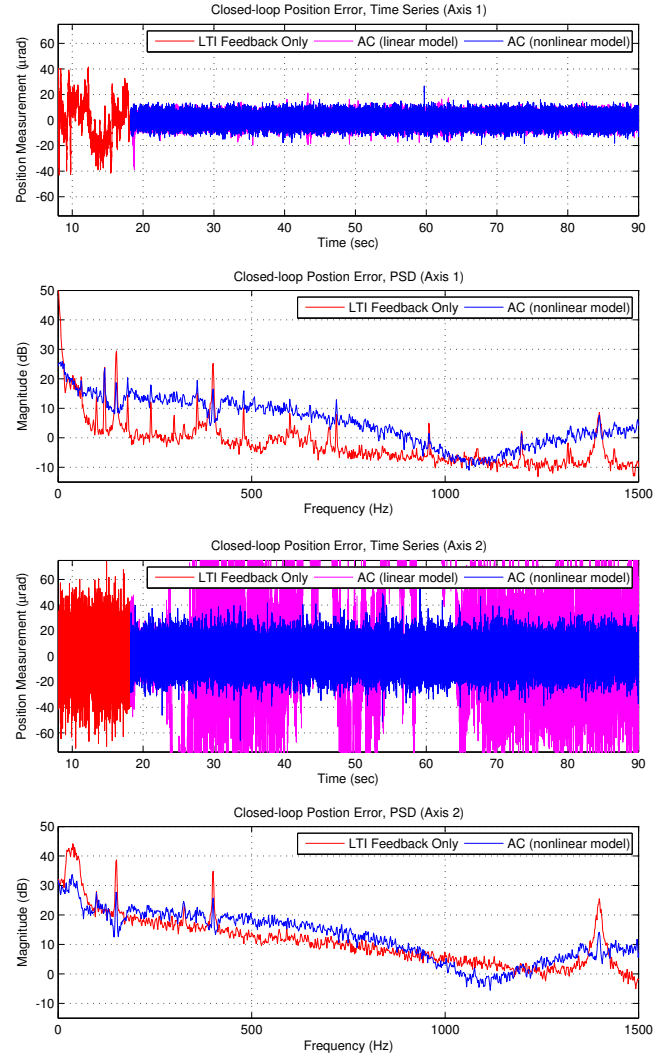


Fig. 6. Output errors  $y$  for two experiments with larger disturbance magnitude. Top: Axis 1 time series and PSDs. Bottom: Axis 2 time series and PSDs. LTI feedback only for  $t \leq 19$  sec. Adaptive control begins at  $t = 19$  sec, with  $\hat{G}$  (linear plant model) or  $\hat{G}_{NL}$  (nonlinear plant model).

TABLE II  
STEADY-STATE RMS OUTPUT POSITION ERRORS  
WITH HIGHER DISTURBANCE MAGNITUDE

Controller	Axis 1	Axis 2	Interval
LTI Feedback Only	16.690 $\mu\text{rad}$	19.582 $\mu\text{rad}$	5–15 sec.
AC with $\hat{G}$	3.334 $\mu\text{rad}$	64.701 $\mu\text{rad}$	25–35 sec.
AC with $\hat{G}_{NL}$	3.806 $\mu\text{rad}$	9.117 $\mu\text{rad}$	25–35 sec.

beam steering, with  $2 \mu\text{rad}$  resolution over a range of  $\pm 300 \mu\text{rad}$  and rapid angle transition within its driver's 3125 Hz update rate. This research suggests that the new device is an alternative to fast steering mirrors in a variety of electro-optical systems. The small liquid crystal device has no mechanical moving parts or flexures that generate resonances, and the device requires low power.

Both linear time-invariant (LTI) feedback and adaptive control have been applied to drive the liquid crystal beam steering device at the driver update rate. The experimental

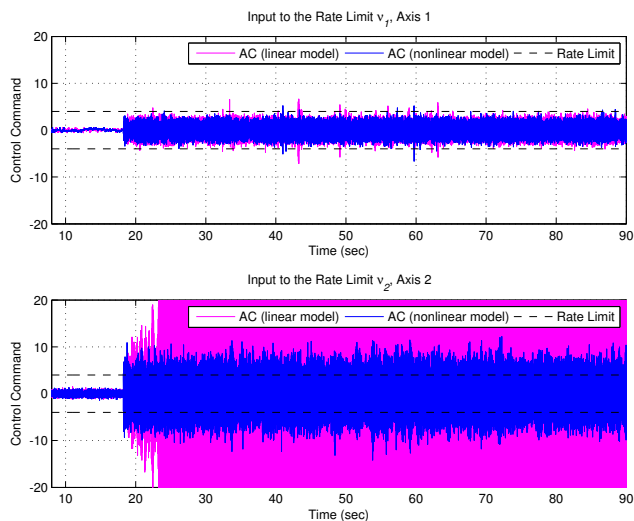


Fig. 7. Comparison of input control commands to the rate limit: adaptive controller based on  $\hat{G}$  (linear plant model) vs. adaptive controller based on  $\hat{G}_{NL}$  (nonlinear plant model). The rate limits are plotted by the black dashed lines.

results illustrate that the adaptive control approach here rejects jitter at frequencies far beyond the bandwidth of an LTI feedback loop, as beam control with mechanical fast steering mirrors [6]–[13].

Two versions of the adaptive controller were considered in this paper. This first version, which is essentially the same as the adaptive controllers in [8]–[13], uses a linear plant model to generate a disturbance estimate. The second version of the adaptive controller, which is new, uses a nonlinear plant model to generate the disturbance estimate. With the liquid crystal beam steering device, the mapping from the control commands to the output beam angle has nonlinearities due to quantization and a rate limit. For sufficiently small disturbance amplitudes, the first version of the adaptive controller adapts to the modeling errors and provides good jitter rejection [16]. However, the experimental results in Section VII show that for sufficiently large disturbance, the earlier version of the adaptive controller is inadequate; the new version of the adaptive controller, which models the plant nonlinearities, provides good jitter rejection over a large range of frequencies.

## REFERENCES

- [1] Roger M. Glaese, Eric H. Anderson, and Paul C. Janzen, "Active suppression of acoustically induced jitter for the airborne laser," *Proc. SPIE, Laser Weapons Technology*, Vol. 4034, SPIE, July 2000, pp. 151–164.
- [2] Mark A. McEver, Daniel G. Cole, and Robert L. Clark, "Adaptive feedback control of optical jitter using Q-parameterization," *Optical Engineering*, Vol. 43, No. 4, April 2004, pp. 904–910.
- [3] L. P. Fowler and R. Blankinship, "Experimental Adaptive Filtering and Disturbance Feedforward Approach for Flexible Beam Train Control with Single Disturbance Path," *2006 Directed Energy Systems Symposium: Beam Control Conference*, DEPS, March 2006.
- [4] Víctor A. Skormin, Mark A. Tascillo, and Timothy E. Busch, "Adaptive jitter rejection technique applicable to airborne laser communication systems," *Optical Engineering*, , No. 5, pp. 1263–1268.
- [5] R. Joseph Watkins, Brij N. Agrawal, Young S. Shin, and Hong-Jen Chen, "Jitter Control of Space and Airborne Laser Beams,"

- International Communications Satellite Systems Conference & Exhibit*, AIAA, Monterey, CA, May 2004.
- [6] Kim, B.-S., Gibson, S., and Tsao, T.-C., "Adaptive control of a tilt mirror for laser beam steering," in *Proc. of the American Control Conference*, Boston, MA, June 2004, pp. 3417–3421.
- [7] Néstor O. Pérez Arancibia, J. S. Gibson, and Tsu-Chin Tsao, "Adaptive control of MEMS mirrors for beam steering," *IMECE2004*, ASME, Anaheim, CA, November 2004.
- [8] Néstor O. Pérez Arancibia, Neil Chen, J. S. Gibson, and Tsu-Chin Tsao, "Adaptive Control of a MEMS Steering Mirror for Suppression of Laser Beam Jitter," *American Control Conference*, IEEE, Portland, OR, June 2005.
- [9] Néstor O. Pérez Arancibia, Neil Chen, J. S. Gibson, and Tsu-Chin Tsao, "Adaptive Control of a MEMS Steering Mirror for Free-space Laser Communications," *Optics and Photonics 2005*, SPIE, San Diego, CA, August 2005.
- [10] Pérez Arancibia, N. O., Chen, N., Gibson, S., and Tsao, T.-C., "Variable-order adaptive control of a microelectromechanical steering mirror for suppression of laser beam jitter," *Optical Engineering*, Vol. 45, No. 10, October 2006, pp. 104206–1–12.
- [11] P. K. Orzechowski, J. S. Gibson, and Tsu-Chin Tsao, "Adaptive Control of Jitter in a Laser Beam Pointing System," *American Control Conference*, IEEE, Minneapolis, MN, June 2006.
- [12] P. K. Orzechowski, J. S. Gibson, and Tsu-Chin Tsao, "Optimal Jitter Rejection in Laser Beam Steering with Variable-Order Adaptive Control," *Conference on Decision and Control*, IEEE, San Diego, CA, December 2006.
- [13] P. K. Orzechowski, J. S. Gibson, and Tsu-Chin Tsao, "Optimal Suppression of Laser Beam Jitter by High-Order RLS Adaptive Control," *IEEE Transactions on Control Systems Technology*, Vol. 16, No. 2, pp. 225–267.
- [14] P. K. Orzechowski, J. S. Gibson, Tsu-Chin Tsao, Dan Herrick, Milind Mahajan, and Bing Wen, "Adaptive Rejection of Optical Jitter with a New Liquid Crystal Beam Steering Device," *Defense and Security Symposium*, SPIE, Orlando, FL, April 2007.
- [15] Dan Herrick, P. K. Orzechowski, J. S. Gibson, Tsu-Chin Tsao, Milind Mahajan, and Bing Wen, "An Alternative Beam Alignment Approach for Tactical Systems," *Directed Energy Systems Symposium: Beam Control Conference*, DEPS, Monterey, CA, March 2007.
- [16] P. K. Orzechowski, *High-performance Adaptive Control of Optical Jitter in Laser Beam Systems*, Ph.D. thesis, University of California, Los Angeles, Los Angeles, CA, 2007.
- [17] J. S. Gibson, C.-C. Chang, and B. L. Ellerbroek, "Adaptive Optics: wavefront correction by Use of Adaptive Filtering and Control," *Applied Optics, Optical Technology and Biomedical Optics*, Vol. 39, No. 16, June 2000, pp. 2525–2538.
- [18] J. S. Gibson, C.-C. Chang, and Neil Chen, "Adaptive Optics with a New Modal Decomposition of Actuator and Sensor Spaces," *American Control Conference*, Arlington, VA, June 2001.
- [19] Yu-Tai Liu and J. S. Gibson, "Adaptive optics with adaptive filtering and control," *American Control Conference*, IEEE, Boston, MA, June 2004.
- [20] Yu-Tai Liu, Neil Chen, and J. S. Gibson, "Adaptive Filtering and Control for Wavefront Reconstruction and Jitter Control in Adaptive Optics," *American Control Conference*, IEEE, Portland, OR, June 2005.
- [21] Yu-Hua Lin, Milind Mahajan, Donald Taber, Bing Wen, and Bruce Winker, "Compact 4 cm aperture transmissive liquid crystal optical phased array for free-space optical communications," Vol. 5892, SPIE, August 2005, pp. 58920C1–10.
- [22] Dong-Feng Gu, Bruce Winker, Donald Taber, Jeff Cheung, Yiwei Lu, Paul Kobrin, and Zhiming Zhuang, "Dual Frequency Liquid Crystal Devices for Infrared Electro-Optical Applications," Vol. 4799, SPIE, 2002, pp. 37–47.
- [23] D. Gu, B. Winker, B. Wen, D. Taber, and A. Brackley, "Wavefront Control with a Spatial Light Modulator Containing Dual-Frequency Liquid Crystal," Vol. 5553, SPIE, 2004, pp. 68–82.
- [24] S.-B. Jiang and J. S. Gibson, "An Unwindowed Multichannel Lattice Filter with Orthogonal Channels," *IEEE Transactions on Signal Processing*, Vol. 43, No. 12, December 1995, pp. 2831–2842.
- [25] B. Widrow and S. D. Stearns, *Adaptive Signal Processing*, Prentice Hall, Englewood Cliffs, NJ, 1985.
- [26] B. Widrow and E. Walach, *Adaptive Inverse Control*, Prentice Hall, Englewood Cliffs, NJ, 1996.